Aust. J. Phys., 1979, **32**, 9–24

Pulsar Microstructure: Periodicities, Polarization and Probes of Pulsar Magnetospheres

J. M. Cordes

Department of Physics and Astronomy, University of Massachusetts, Amherst, Massachusetts 01003, U.S.A.

Abstract

This paper discusses characteristic time scales, periodicities and polarization of microstructure in pulsar signals. The relationship of microstructure polarization to the polarization of subpulses and the average profile is analysed in detail for PSR 2016+28. For this pulsar the contributions of micropulses to the variance of the intensity vary with radio frequency ν approximately as ν^{-1} and the characteristic time scale varies as $\nu^{-\alpha}$, with $0{\cdot}2 \lesssim \alpha \lesssim 0{\cdot}3$. In summarizing possible interpretations of microstructure, we distinguish between angular beaming and temporal modulation processes that can cause intensity variations. We outline, with regard to the frequency dependence of pulse structure, how micropulses can be used to probe the depth and variability of the emission region.

Introduction

It is generally understood that pulsar radiation is due to rotation of highly magnetized neutron stars and that the average pulse width is related to the angular width of a beam pattern. The small duty cycle and polarization of pulses suggest that radiation occurs near the magnetic pole of a skewed, approximately dipolar field (Radhakrishnan and Cooke 1969). A close look at single pulses reveals a number of details which have yet to be understood in this, or any, pulsar radiation model. We discuss here the shortest structure seen (the microstructure), which has characteristic time scales of about one milliperiod, and consider the latest observational results on the characteristic widths, periodicities, spectra and polarization of microstructure. We point to ways in which microstructure can be interpreted within the Radhakrishnan and Cooke model while distinguishing between micropulses as due to small angular beams or to true temporal fluctuations of the radiation. Uses of microstructure as a probe of the emission region are outlined, including its use in resolving whether different radio frequencies are emitted at different altitudes.

Pulse Constituents

When one looks at a single pulse from a typical pulsar, three constituents are obvious. The pulse from pulsar PSR 0950+08 in Fig. 1* shows *subpulses* with typical widths of a few milliseconds and narrow intense spikes or *micropulses* of $\sim 200\ \mu$s

* All data discussed in this paper were obtained at Arecibo Observatory (NAIC). Distortion of signals due to dispersion in the interstellar medium was removed either by the software technique of Hankins (1971) or by using a hardware post-detection de-disperser (Boriakoff 1973).

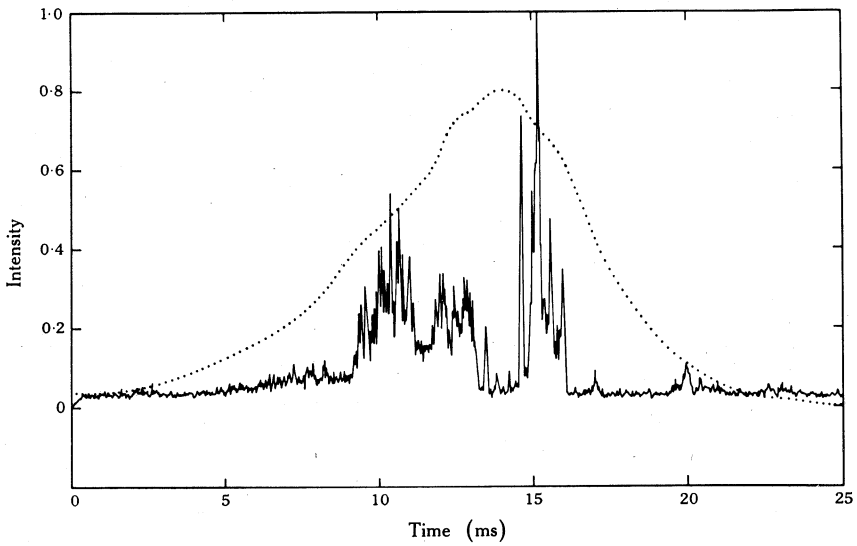

Fig. 1. Single pulse from PSR 0950+08 at 430 MHz plotted with 26 μs time resolution. The dotted curve is the average of several hundred pulses.

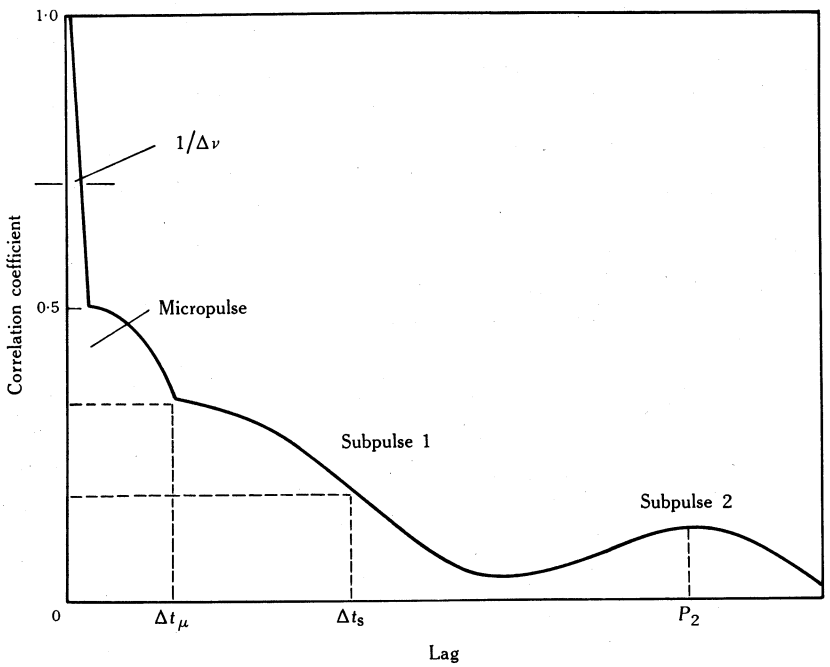

Fig. 2. Schematic autocorrelation function (ACF) of the intensity. Various time scales are obtained from the ACF, including the micropulse break point Δt_μ, the subpulse half-width at half-maximum Δt_s and the secondary subpulse feature centred on a lag P_2. The narrow spike near zero lag has a width equal to the reciprocal of the receiver bandwidth $\Delta\nu$. The amplitude of the zero-lag spike is 0·5 if the intensity is from a single receiver channel and if the pulsar signal is amplitude-modulated gaussian noise (see text).

duration. Single pulses are modulated by a window function that is revealed by summing a large number ($\sim 10^3$) of pulses to form a *mean intensity profile* (also called average pulse profile or average waveform). The profile represents, in part, a multiplicative factor of single pulse emission because regions of high intensity in average profiles correspond to pulse longitudes where the strongest subpulses usually occur. However, low-intensity regions show occasional strong subpulses, signifying that the profile is also a measure of the frequency of occurrence of subpulse emission.

The distribution of average profile shapes and widths among the pulsars suggests that (1) its multiplicative aspect is due to an angular beam pattern that rotates through the line of sight, and (2) the beam pattern is probably a hollow cone centred on an axis of symmetry; e.g. a magnetic pole. Most pulsars have average profile widths that are roughly 5–10 % of their pulse period. There are exceptions to this, however, and Backer (1976) has shown that a single physical beam shape is not sufficient to explain the observed profile shapes and widths, unless nonrandom configurations of the rotation axis and magnetic axis occur. The important conclusions, however, are that the average profile is related to a beam shape and that average profile shapes are constant over several-year time scales, suggesting an association with a strong magnetic field.

Micropulses and Subpulses

The structure in single pulses varies dramatically from pulse to pulse. Except for drifting subpulses, there are no apparent pulse to pulse correlations of the structure. It is convenient to view the single pulse intensity as one realization of a random process. To quantify the characteristic time scales and relative strengths of subpulses and micropulses, we have computed the average autocorrelation function (ACF) of the intensity by summing several hundred single-pulse ACFs. A schematic ACF is shown in Fig. 2 which identifies features associated with microstructure and subpulses, as well as a feature near zero lag that represents the autocorrelation of the noise aspect of the pulsar signal, which decorrelates on an inverse bandwidth time scale. We characterize the subpulse width by taking the half-width at half maximum of the roughly gaussian-shaped feature centred on zero lag. The characteristic separation of subpulses, particularly evident for drifting-subpulse pulsars, is given by the lag of the peak of a second subpulse feature. Micropulses are manifested by a narrow feature that sits atop the first subpulse feature and whose width we measure by identifying a break point in the ACF; this corresponds roughly to taking the e^{-2} width.

In Fig. 3 the so-obtained micropulse (Δt_μ) and subpulse (Δt_s) widths are plotted against pulse period for 10 pulsars at an observation frequency of 430 MHz. Two pulsars, namely PSR 0525+21 and 1237+25, did not show micropulse features in ACFs but the former displays occasional micropulse-like structure with a 3 ms time scale. Table 1 lists the values of Δt_s and Δt_μ.

Subpulse and micropulse widths both tend to increase with pulse period P. From a larger sample of pulsars, Taylor *et al.* (1975) have found the subpulse scale to vary, albeit with a large amount of scatter, roughly as

$$\Delta t_s \approx 7 \times 10^{-3} P. \quad (1)$$

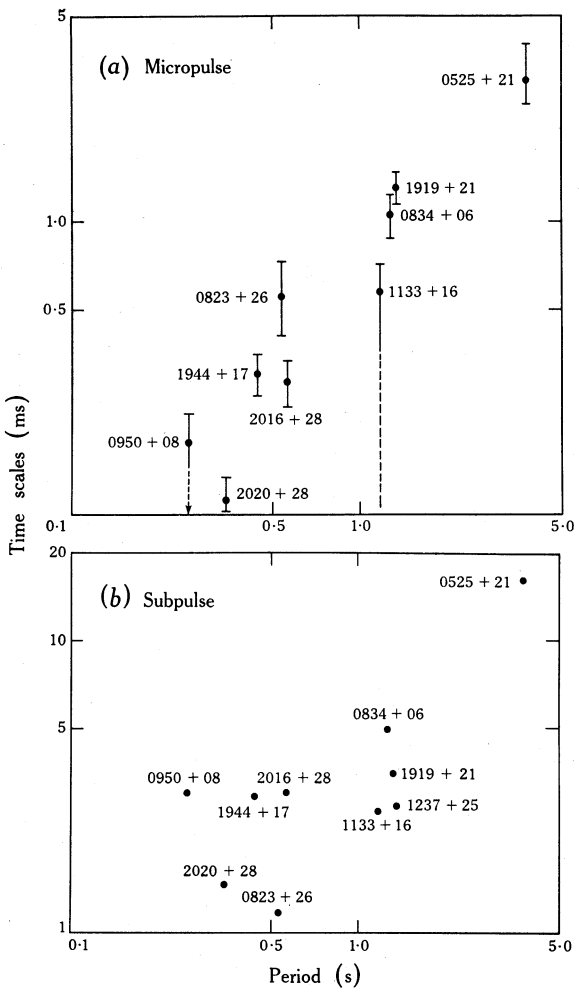

Fig. 3. Micropulse (*a*) and subpulse (*b*) time scales plotted against pulse period. The dashed lines in (*a*) show the range of micropulse time scales seen in single pulses from pulsars PSR 0950+08 and 1133+16.

Table 1. Subpulse and micropulse time scales

Pulsar No.	Width[A] Δt_s (ms)	Width[B] Δt_μ (ms)	Pulsar No.	Width[A] Δt_s (ms)	Width[B] Δt_μ (ms)
0525+21	16	3·00	1237+25	2·7	—
0823+26	1·2	0·55	1919+21	3·5	1·30
0834+06	5·0	1·05	1944+17	2·9	0·30
0950+08	3·0	0·18	2016+28	3·0	0·28
1133+16	2·6	0·58	2020+28	1·5	0·11

[A] Measured from ACFs as the half-width at half-maximum of the subpulse feature.
[B] Measured at the break point in the ACF, except for PSR 0525+21 which was determined from micropulses in single pulses.

(Note that the numerical factor in equation (1) differs from that given by Taylor *et al.* because of the difference in definition of subpulse time scale.) The micropulse scale varies approximately as

$$\Delta t_\mu \approx 10^{-3} P. \tag{2}$$

The scatter about this relation also is large, especially since micropulse widths vary over at least an order of magnitude for pulsars PSR 0950+08 and 1133+16 (Hankins 1972). However, it appears that most micropulses from PSR 0950+08 are well resolved with a resolution of 0·8 μs (Hankins and Boriakoff 1978).

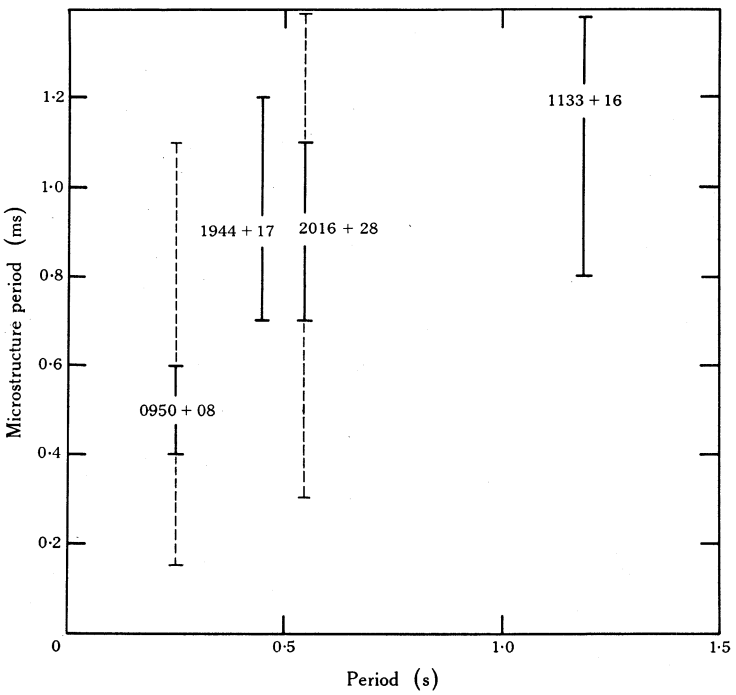

Fig. 4. Periods of the microstructure periodicity plotted against main pulse period. The dashed lines represent the observed range of periods for PSR 0950+08 and 2016+28. The periods for PSR 1133+16 and 1944+17 may vary over larger ranges than indicated.

Linear relationships of subpulse and micropulse width with pulse period would be expected if narrow beams were responsible for subpulses and micropulses and if the beam width were independent of pulse period. Nonlinear relationships may imply that the beam size is itself a function of pulse period. However, it is possible that subpulses and/or micropulses are due to temporal modulations of the emission region that would be seen by an observer corotating with the star. The model of Ruderman and Sutherland (1975), for example, predicts modulations of particle injection at the stellar surface that might be observable as intensity variations. Because such modulations are dependent on rotation-generated electric fields, a variation with pulse period of micropulse durations may also be expected. Thus, the question is open at this point as to whether subpulses and micropulses are due to angular beams or temporal modulations.

Micropulse Periodicities

Microstructure from a few pulsars has been observed to be quasi-periodic. PSR 2016+28 has microstructure in most single pulses that is quasi-periodic with an average period of 0·9 ms (Boriakoff 1976; Cordes 1976*b*), although this period varies over a range from 0·3 to 2·0 ms. There is no correlation for the microstructure period in adjacent drifting subpulses, nor is there any strong correlation of the microstructure of a drifting subpulse from one pulse period to the next. PSR 1944+17, another pulsar with drifting subpulses, also has a fairly systematic micropulse periodicity with an average period of 0·9 ms. The pulsars PSR 1133+16 and 0950+08 show more transient periodicities than do 2016+28 and 1944+17. A period for the microstructure of PSR 1133+16 of about 1·2 ms at 430 MHz (Cordes and Hankins 1977) is considerably larger than the 0·15 ms period found by Ferguson *et al.* (1976) at 1420 MHz. However, the 0·15 ms period was found in only one pulse and may or may not be representative. Generally, the resonant Q of the micropulse periodicity is small. Up to 10 cycles of the periodicity are seen in a given subpulse of PSR 2016+28, implying $Q = 10$. The micropulse periods for four pulsars are plotted against pulse period in Fig. 4.

Pulsar Signal as Amplitude-modulated Shot Noise

Upon obtaining intensity autocorrelation functions, a statistical model for the pulsar signal was desired to explain features seen in the ACFs. Rickett (1975) proposed an amplitude-modulated noise model for the narrow-band pulsar signal. When the IF receiver signal is shifted to zero frequency, the resultant base-band signal $\varepsilon(t)$ can be written (before detection) as

$$\varepsilon(t) = a(t)n(t), \tag{3}$$

where $n(t)$ is a complex noise-like random process and $a(t)$ is a stochastic envelope that describes all variations of the signal, including micropulses, subpulses and the average profile. One can assume statistical properties for $n(t)$ and test their consistency with actual data. It can be shown that the normalized intensity ACF is of the form

$$r_I(\tau) = r_A(\tau)\{1+m^2\Delta(\tau)\}/(1+m^2), \tag{4}$$

where $r_A(\tau)$ is the ACF of $A(\tau) \equiv a^2(\tau)$ and $\Delta(\tau)$ is the correlation function of the noise and is essentially the ACF of the response of the receiver to an impulse. The modulation index m is unity if $n(t)$ is complex gaussian noise. The height of the spike-like term $\Delta(\tau)$ in the measured ACF can be compared with that predicted by the model for gaussian noise. Measurements of PSR 2016+28 (Cordes 1976*a*) and of PSR 0950+08 (Hankins and Boriakoff 1978) show consistency of the data with gaussian noise.

Cordes (1976*b*) has discussed the significance of the consistency with gaussian noise and in particular has derived possible ways in which deviations from gaussian noise might occur. In the curvature radiation model of Radhakrishnan and Cooke (1969), it is most likely that a single coherently radiating emitter of particles will produce a very short nanosecond duration pulse. Micropulses and subpulses are therefore ensembles of such 'nanopulses' and the question arises as to what is the typical spacing of these nanopulses. The best time resolution obtained to date is 0·8 μs; consistency of the data with gaussian noise with this resolution implies that a large number of

nanopulses must occur in a $0{\cdot}8\ \mu$s interval. Hence, by the central limit theorem, the signal is modulated gaussian noise. Interstellar scattering can produce gaussian noise from shot noise, but for PSR 0950+08 at 430 MHz, the scattering broadening time is $\ll 0{\cdot}8\ \mu$s. Therefore the viable conclusion is that the observed signal arises from the incoherent addition of contributions from a large number of coherent emission regions. Physically, this means that the process that causes coherence (plasma instabilities) produces a large number of coherently radiating regions, rather than a few isolated ones. Moreover, the coherence mechanism is probably decoupled from that which determines micropulse durations because the ratio of relevant time scales is $(10^{-4}\ \text{s})/(10^{-9}\ \text{s}) \approx 10^5$.

Spectral Properties of Microstructure and Subpulses

Microstructure from PSR 0950+08 has been detected over the range of frequencies from 111 MHz to 3 GHz. However, simultaneous multifrequency measurements have been fairly sparse. Rickett *et al.* (1975) cross-correlated microstructure between 111 and 318 MHz and obtained a 50% lower limit on the correlation coefficient. Recently, Bartel (1978) has found large correlation over a 20 MHz range near 3 GHz. The spectral structure of micropulses over small frequency ranges has also proved to be consistent with the amplitude-modulated noise model for PSR 0950+08. From the model, one would expect to see frequency structure with a characteristic width equal to the inverse micropulse width. Rickett *et al.* (1975) detected such structure and recently Cordes and Hankins (1979) have analysed frequency structure (over a $1{\cdot}25$ MHz bandwidth centred on 430 MHz) and verified that it has a ratio of the standard deviation to the mean of unity, as expected from the noise model.

The strength of microstructure, namely its contribution to the variance of the intensity, can be measured from the intensity ACF. We define the microstructure modulation index m_μ as the ratio of the standard deviation of the micropulse intensity to the mean:

$$m_\mu = \sigma_{I\mu}/\langle I_\mu \rangle . \tag{5}$$

Letting H_μ and H_s be the respective amplitudes of the micropulse and subpulse features in the ACF, the modulation index is $m_\mu = (H_\mu/H_s)^{\frac{1}{2}}$. Fig. 5*a* shows ACFs for PSR 2016+28 at three frequencies. Normalization was arbitrarily chosen so that the subpulse level of correlation (e.g. lags $\gtrsim 0{\cdot}4$ ms) is the same at the three frequencies. The amplitude of the microstructure feature at 606 MHz is clearly smaller than at 318 and 430 MHz and reflects a frequency dependence of the microstructure modulation index. The ACFs in Fig. 5*b* (out to a lag of 15 ms) include 1410 MHz for which the microstructure feature is not evident. Table 2 lists values of m_μ at the four frequencies for PSR 2016+28. Above a frequency of 430 MHz, m_μ falls off faster than ν^{-1}. Microstructure for several other pulsars (PSR 1919+21, 1944+17) also diminishes with increasing frequency.

Therefore, although micropulses seem to be highly correlated between 318 and 111 MHz for PSR 0950+08, microstructure apparently has a narrower total spectral range than does the total flux emitted by a pulsar. Pulsars in general may behave similarly to PSR 1919+21, which evidently has two components of emission: a drifting subpulse component that exhibits microstructure at low frequencies ($\lesssim 200$ MHz) and a nondrifting amorphous component of emission that dominates at higher frequencies (Cordes 1975).

Average profile widths for many pulsars and subpulses for a few pulsars are weakly dependent on frequency approximately as $\nu^{-0.25}$ (Sieber 1973; Taylor *et al.* 1975; Backer 1976). A similar dependence evidently may cause the difference in shapes of the ACFs in Fig. 5*b*. The valley between the two subpulse features at 430 MHz is filled in at 606 and 1410 MHz. Two interpretations of this can be made. The first is that P_2, the separation between subpulses, may vary with frequency as it does for PSR 0031−07 and 0809+74 with a $\nu^{-0.25}$ dependence (Taylor *et al.* 1975). If so, then the valley will become shallower only if subpulse widths remain constant or increase with increasing frequency. If subpulse width and separation vary identically with frequency, the valley will not become filled in. A second interpretation is that a nondrifting component of emission becomes important at the higher frequencies,

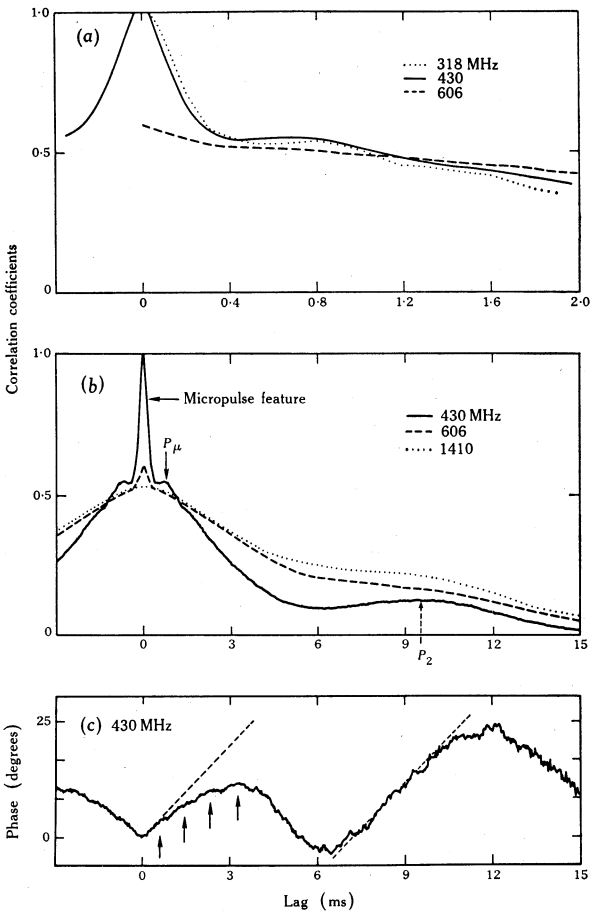

Fig. 5. Autocorrelation functions of PSR 2016+28 at four frequencies: (*a*) 318, 430 and 606 MHz for lags <2 ms, and (*b*) 430, 606 and 1410 MHz for lags out to 15 ms. The signals at 318, 606 and 1410 MHz were from nominally linearly polarized feeds. The 430 MHz ACF shown is of the complex Stokes parameter $L = Q + iU$, and its phase is shown in (*c*). In (*b*), P_μ denotes a feature due to a 0·9 ms periodicity in microstructure. In (*c*), arrows point to ripples in the phase that are periodic with a 0·9 ms period; the dashed lines in this figure indicate the phase rotation expected from the position angle rotation of the average profile in Fig. 6.

as has been found for PSR 1919+21 (Cordes 1975). A nondrifting component, of broader width than the drifting subpulses, would tend to smear out the subpulse features of the ACF and is consistent with the ACFs showing a correlation at 15 ms lag that increases with frequency.

Table 2. Microstructure strength and width for PSR 2016+28

Frequency ν (MHz)	Strength m_μ	Width[A] $\Delta t_{\mu\frac{1}{2}}$ (μs)
318	0·92	170
430	0·87	160
606	0·39	135
1410	<0·14	—

[A] Half-width at half-maximum of feature in ACF.

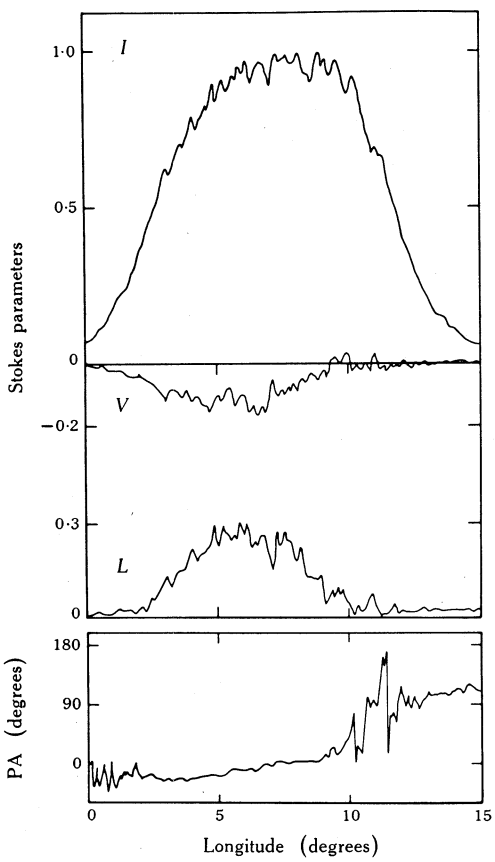

Fig. 6. Average Stokes parameters of 300 pulses from PSR 2016+28 at 430 MHz. The position angle (PA) has an arbitrary reference angle.

Little is known about the variation of micropulse widths with frequency. Hankins (1972) and Cordes and Hankins (1973) found no obvious variation with frequency of the autocorrelation break-point lag for PSR 0950+08 or 1133+16, but measurement errors may have disguised a $\nu^{-0\cdot25}$ frequency dependence. Observations at higher

frequencies have not resolved the issue for PSR 1133+16 because there are evidently two characteristic micropulse time scales and, moreover, occasional very strong pulses tend to dominate the ACFs for that pulsar. Recently obtained results for PSR 2016+28 suggest a $\nu^{-\alpha}$ variation of the micropulse time scales in Table 2, with $0{\cdot}2 \lesssim \alpha \lesssim 0{\cdot}3$.

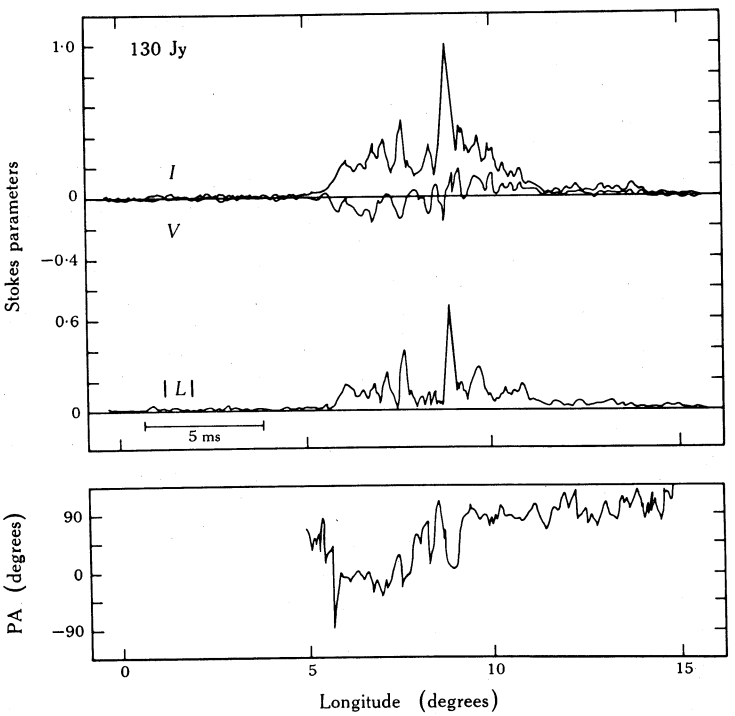

Fig. 7. Stokes parameters of a single pulse from PSR 2016+28 at 430 MHz. The horizontal bar represents 5 ms of time. The position angle (PA) is plotted only where the signal to noise ratio is above a certain threshold.

Polarization

Radhakrishnan and Cooke (1969) proposed that the average position angle rotation for the Vela pulsar is geometric in origin and, in particular, arises from the changing orientation of the projected magnetic field onto the plane of the sky. This model is quite accurate for most pulsars in spite of the appearance of nonmonotonic and discontinuous position angle rotations for some pulsars. Such counter examples can be reconciled with the model by taking into account the preference of the position angle for one of two orthogonal values (Manchester *et al.* 1975). Each of these orthogonal modes rotates with pulse longitude in the geometric manner and discontinuities occur at longitudes where the modes are equally probable (Backer *et al.* 1976; Cordes *et al.* 1978).

Fig. 6 shows the average Stokes parameters of 300 pulses from PSR 2016+28. The position angle rotates smoothly for the first 10° of longitude, then rotates quickly and erratically through 90°, and then again rotates smoothly. The quick rotation through 90° occurs where the two orthogonal modes are roughly equally probable.

For longitudes greater than 10°, the frequencies of occurrence of both modes are comparable, thus causing the magnitude of the linear polarization to be small.

Polarization measurements of microstructure are difficult to make with the required high time resolution. The competing goals of minimizing both dispersion distortion and estimation errors have led us to an autocorrelation analysis of the Stokes parameters. The necessity for some such averaging procedure is clear from the single pulse Stokes parameters for PSR 2016+28 in Fig. 7. The circular and linear polarization and the position angle show as much variability on short time scales as does the total intensity. It is both tedious and risky to attempt to conclude much from the behaviour of single pulses.

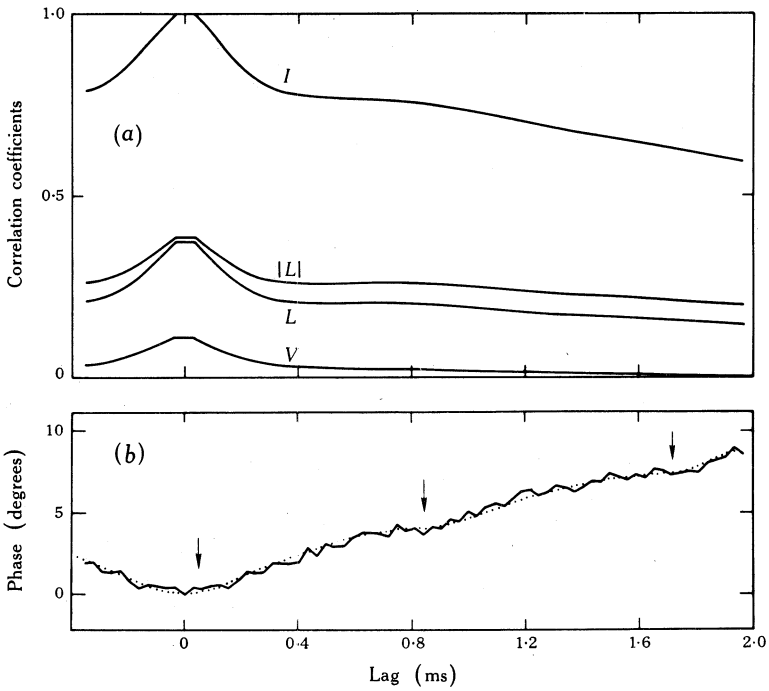

Fig. 8. Autocorrelation functions of the Stokes parameters of PSR 2016+28 at 430 MHz, computed by summing the ACFs of 300 single-pulse Stokes parameters. The zero-lag spike due to noise has been removed, thus causing the flat-topped peaks of the curves. All ACFs were normalized by the zero lag of the ACF of the total intensity *I*. The dotted curve through the phase in (*b*) was drawn to accentuate the flattening of the phase curve near zero lag and at lags near 0·9 and 1·8 ms.

Fig. 8 shows ACFs of the Stokes parameters averaged over 300 pulses. Two ACFs were computed for the linear polarization. The ACF of $L(t) = Q(t)+iU(t)$ is complex and therefore both the magnitude and phase are shown in Fig. 8. The ACF of the magnitude $|L(t)|$ was also computed. The squared-off appearance of the ACFs at zero lag is because of removal of the zero-lag spike due to noise. All ACFs were normalized relative to the zero-lag value for the total intensity. Therefore the zero-lag amplitudes of the ACFs of L and V yield the mean square values of the degree of linear and of circular polarization respectively. We find that linear and circular polarization of microstructure have r.m.s. degrees of polarization of 61% and 34%

respectively. The width of the microstructure feature is the same for all the ACFs but the amplitude is different. In particular, V, L and $|L|$ decorrelate from their peak values by greater amounts on the micropulse time scale than does the total intensity I. Moreover, L decorrelates more than $|L|$ on the micropulse time scale. The conclusions that can be made from this are that:

(1) the state of polarization varies (at most) slowly over the micropulse duration;
(2) the state of polarization, especially the sign of circular polarization and the position angle, must often change significantly on the edges of micropulses.

The polarization transitions that occur on micropulse edges appear to be in the form of jumps between two orthogonal position angles and zero-crossings of the circular polarization (i.e. changes from left-hand to right-hand circular polarization and vice versa). The transition time is difficult to establish but is certainly smaller than the micropulse duration. The transitions on micropulse edges resemble position-angle rotations of 90° that occur on subpulse peripheries. In that regard, micropulses look like shorter duration subpulses. Recently, Cordes *et al.* (1978) have shown that a positive value of the Stokes parameter V is almost always associated with only one of the orthogonal position angles for PSR 2020+28. This result establishes that two truly orthogonal modes of polarization are emitted by the pulsar. The frequency of occurrence of each mode is a strong function of pulse longitude as well as being variable from pulsar to pulsar.

Relationship of Micropulse Polarization to Average Polarization

The position angle is an important diagnostic tool for determining the nature of micropulses and subpulses. The question is whether the position angle rotates through subpulses and micropulses in the same geometric fashion as it does in average profiles. If so then, for example, a micropulse is due to emitters that span an azimuthal (around the magnetic pole) range of magnetic field lines. A micropulse would therefore be due to tiny angular radiation beams that represent transient structure in the overall average-profile beam. If, on the contrary, the position angle is constant through a micropulse, then a micropulse may be produced by particles that are at the *same* azimuthal angle with respect to the magnetic pole.

Our best handle on the variation of position angle on short time scales is the phase of the ACF of the linear polarization. Formally, we can write this ACF as

$$R_L(\tau) = |R_L(\tau)| \exp\big(i\psi(\tau)\big) \equiv \int dt\, L^*(t)\, L(t+\tau)$$

$$= \int dt\, |L(t)|\, |L(t+\tau)| \exp\big\{2i\big(\phi(t+\tau)-\phi(t)\big)\big\}, \qquad (6)$$

where $\phi(t) = \frac{1}{2}\arctan\{U(t)/Q(t)\}$ is the usual position angle. For some pulsars, the position-angle rotation through the average pulse is approximately linear at a rate, say, of α degrees ms^{-1}. For linear rotation, the phase of $R_L(\tau)$ should also rotate linearly with lag,

$$\psi(\tau) = 2\alpha\tau, \qquad (7)$$

as long as the position angle rotates linearly on all time scales. The phase of the ACF of L shown in Fig. 5*c* out to a lag of 15 ms clearly does not rotate linearly with lag.

Dashed lines in this figure show the slope and sense of phase rotation anticipated from the position-angle rotation of the average profile (namely $\alpha \sim 6{\cdot}6\,\mathrm{deg\,ms^{-1}}$). The actual phase rotates linearly around zero lag to 2 ms lag, then it changes direction from 3 to about 6 ms, rotates linearly again from 7 to 11 ms and changes direction again. The linear segments of the phase rotation are consistent with a geometric-style position-angle rotation through the majority of the subpulse duration. The phase reversals at 3 and 12 ms are most likely due to the transitions between orthogonal angles that occur on subpulse peripheries. At a lag of 3 ms, the correlation function essentially compares the position angles of the leading (the earlier) and trailing edges of subpulses, which are often 90° apart. Between 7 and 11 ms, the trailing edge of the first subpulse is compared with the leading edge of the second subpulse and, at lags greater than 12 ms, the leading edge of the first subpulse is compared with the trailing edge of the second subpulse. The phase implies that the leading edge of the first subpulse and the trailing edge of the second subpulse often (but not necessarily always) have position angles of the same mode.

On micropulse time scales the phase shows a weak periodicity (with $\sim 0{\cdot}9$ ms period) in Fig. 5*c*, as indicated by the arrows. The higher resolution plot of the phase in Fig. 8*b* again shows the periodicity in the phase. This latter figure suggests (but, I admit, is not very convincing) that the phase may be constant at lags less than $\sim 100\,\mu$s. This effect is more noticeable in the ACFs computed separately for the second half of the average profile (Cordes and Hankins 1977). We shall regard the constancy of the phase as merely a possibility whose proof will require additional observations but whose implications we nonetheless will discuss in the next section. The periodicity in the phase with the micropulse period might be produced in two ways. The first is that the position angle may rotate at the average-profile rate in micropulses, but transitions between orthogonal modes cause phase reversals analogous to those on subpulse time scales. Secondly, the position angle may be constant in a micropulse but rotates between micropulses; then the position angle is more like a 'staircase' than a ramp. Neither interpretation can be rejected here and in the next section we will take full advantage of this latitude.

Interpretation of Micropulses and Subpulses

We assume here that the polarization position angle of the average profile is determined, as in the Radhakrishnan and Cooke (1969) model, by the magnetic field lines to which the observer's line of sight is tangential. We infer, then, that subpulses are most likely related to sub-beams within the overall radiation beam because, apart from fast rotations between orthogonal angles, the position angle rotates through subpulses as it does through the average profile. The angular size of the subpulse beam must vary with pulse period in order that the subpulse widths approximately obey equation (1) above.

Micropulses may be due either to beams similar to subpulse beams, to retardation delays over a radial range or to true temporal modulations. If the position angle ultimately proves to rotate through micropulses as it does on longer time scales, then micropulses can be interpreted as beams of plasma within a bundle of field lines. The total angle swept by the position angle is then related to the range of azimuthal angle encompassed by the plasma beam.

If, on the contrary, the position angle is indeed constant within a micropulse, then a micropulse is produced by particles at the same azimuthal angle. Particles in a

very narrow plasma tube can cause micropulses in this way, where the micropulse width is the light-travel time corresponding to the length of the tube. A variation on this theme is that radiation only occurs when plasma reaches a particular radius. In that case, the beamwidth of curvature radiation may be observable as the micropulse duration. Particles moving along a curved trajectory radiate in a beam whose angular width $\Delta\phi$ transverse to the plane of trajectory is given by

$$\Delta\phi \approx \gamma^{-1}(\nu/\nu_c)^{-\frac{1}{3}}, \tag{8}$$

for frequencies less than the critical frequency $\nu_c \sim \gamma^3 c/\rho$, where ρ is the radius of curvature and γ is the Lorentz factor (Jackson 1962). This model produces microstructure with amplitude-modulated noise properties because an observer sees a sequence of narrow pulses with width $\delta t \sim \nu_c^{-1} \approx 1$ ns for $\gamma = 10^3$ and $\rho \sim 10^{10}$ cm (Ruderman and Sutherland 1975). The amplitude modulation of the narrow pulses has a time duration $\Delta t \sim \Delta\phi/\dot{\phi}$, where $\dot{\phi}$ is the derivative of the azimuthal angle of the observer's line of sight. If the line of sight does not pass very close to the magnetic pole, then $\dot{\phi} \approx \Omega = 2\pi/P$, where P is the pulse period as before, and therefore

$$\Delta t_\mu \sim (P/2\pi\gamma)(\nu/\nu_c)^{-\frac{1}{3}}. \tag{9}$$

For $\gamma = 10^3$ we get $\Delta t_\mu \sim 160\, P(\nu/\nu_c)^{-\frac{1}{3}}$ μs, which is remarkably similar to the value and frequency dependence observed for PSR 2016+28.

Our discussion here is intended to be exploratory and it is acknowledged that the entire issue of post-emission propagation effects has been blissfully ignored. The point of view taken is that the polarization position angle is determined, within a 90° uncertainty, by the ambient stellar field. Transitions between orthogonal angles may be a post-emission effect, but the tendency for them to occur on subpulse and micropulse edges suggests a radiative transfer effect in the emission region. Apart from transitions between orthogonal angles and large amounts of circular polarization, there are no observations that definitively imply that radiative transfer effects are important.

Microstructure as a Probe of the Emission Region

The interpretation of micropulses and subpulses is ultimately related to the question of whether all radio frequencies are emitted at the same altitude. Our discussion here will assume that radiation is emitted tangentially to magnetic field lines along which particles are streaming relativistically. Several theoretical treatments (Komesaroff 1970; Ruderman and Sutherland 1975; Benford and Buschauer 1977) have assumed or demonstrated that the approximate $\nu^{-0.25}$ dependence of average profile widths results from higher frequencies being radiated closer to the star than low frequencies. The contraction of average profiles with frequency is therefore directly related to the flaring of the field lines near a magnetic pole, as shown schematically in Fig. 9. Cordes (1978) has recently shown that if radio frequencies are radiated differentially, then approximately a 5 : 1 ratio of radii is needed to account for the average profile shape of PSR 1133+16 from 40 to 1400 MHz.

Differential radiation will cause low frequency pulses to arrive earlier than high frequency pulses because of retardation and corotation aberration. Craft (1970) found that the midpoint between the lobes of the average profiles of PSR 0525+21,

0950+08 and 1133+16 was the proper fiducial point for making dispersion measurements, which would not be the case if retardation and aberration were significant. Therefore the lowest observed frequencies are emitted no further than a few per cent of the radius of the velocity-of-light cylinder (Cordes 1978).

The $\nu^{-0.25}$ dependence of average-profile widths may be otherwise produced, however. In fact, all frequencies may be radiated simultaneously at the same radius such that the $\nu^{-0.25}$ dependence is caused by a systematic variation of the radiated spectrum with perpendicular distance from the magnetic pole.

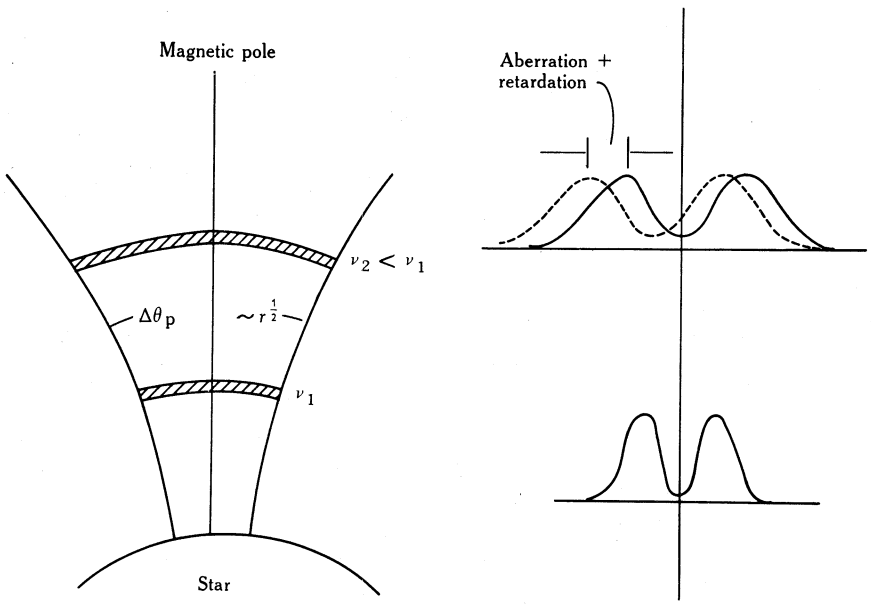

Fig. 9. Schematic diagram of the magnetic field line configuration that is relevant to one class of models. The angular separation of two field lines varies with radius as shown and can cause the average pulse profile at a frequency $\nu_1 > \nu_2$ to be narrower than the profile at ν_2. If the two frequencies are radiated at two radii that differ substantially then the low frequency pulse will arrive earlier than the high frequency one because of aberration and retardation.

Microstructure can be used to test the variable-radius model against the constant-radius model. If radiation is produced at different altitudes for different frequencies, then the radiation at any given altitude must have a bandwidth much narrower than the total bandwidth. Micropulses may then be seen over a large bandwidth, but the spectrum of a single micropulse will probably be heavily modulated because the radiation efficiency at different frequencies may be quite different. If all frequencies are emitted at the same radius then a micropulse spectrum will not be heavily modulated (unless post-emission effects, which we are conveniently ignoring here, drastically influence the radiation). A cross-correlation analysis of micropulses at two frequencies can test whether or not micropulse separations vary as $\nu^{-0.25}$, which might be expected if micropulses are due to tubes of plasma that are tied to the magnetic field lines. With the assumption that different frequencies arise from different radii, micropulses may expand away from some fiducial longitude by an amount proportional to $\nu^{-0.25}$. The lag of peak cross-correlation for a single micropulse is then a function of pulse longitude. The fiducial longitude can be identified

as that where the rate of change of the lag of peak correlation is a minimum. For large frequency separations, the cross-correlation coefficient will be small because the micropulses in a sequence will not align at the same lag if micropulse separations vary as $\nu^{-0.25}$.

Measurements such as those outlined above may be realized at Arecibo where a broad-band feed will allow observations of single pulses over a broad frequency range.

Acknowledgments

The author thanks T. H. Hankins and V. Boriakoff for supplying data in advance of publication and gratefully acknowledges discussions with P. Backus, B. J. Rickett, E. Tademaru and J. H. Taylor. Research at the University of Massachusetts is supported by NSF Grant No. AST75–23581. Arecibo Observatory is operated by Cornell University under contract with the NSF. This paper is contribution number 270 of the Five College Observatories.

References

Backer, D. C. (1976). *Astrophys. J.* **209**, 895.
Backer, D. C., Rankin, J. M., and Campbell, D. B. (1976). *Nature* **263**, 202.
Bartel, N. (1978). *Astron. Astrophys.* **62**, 393.
Benford, G., and Buschauer, R. (1977). *Mon. Not. R. Astron. Soc.* **179**, 189.
Boriakoff, V. (1973). Ph.D. Thesis, Cornell University.
Boriakoff, V. (1976). *Astrophys. J. Lett.* **208**, L43.
Cordes, J. M. (1975). *Astrophys. J.* **195**, 193.
Cordes, J. M. (1976*a*). *Astrophys. J.* **208**, 944.
Cordes, J. M. (1976*b*). *Astrophys. J.* **210**, 780.
Cordes, J. M. (1978). *Astrophys. J.* **222,** 1006.
Cordes, J. M., and Hankins, T. H. (1973). *Bull. Am. Astron. Soc.* **5**, 18.
Cordes, J. M., and Hankins, T. H. (1977). *Astrophys. J.* **218**, 484.
Cordes, J. M., and Hankins, T. H. (1979). *Astrophys. J.* (in press).
Cordes, J. M., Rankin, J. M., and Backer, D. C. (1978). *Astrophys. J.* **223,** 961.
Craft, H. D., Jr (1970). Ph.D. Thesis, Cornell University.
Ferguson, D. C., Graham, D. A., Jones, B. B., Seiradakis, J. H., and Wielebinski, R. (1976). *Nature* **260**, 25.
Hankins, T. H. (1971). *Astrophys. J.* **169**, 487.
Hankins, T. H. (1972). *Astrophys. J. Lett.* **177**, L11.
Hankins, T. H., and Boriakoff, V. (1978). *Nature* **276,** 45.
Jackson, J. D. (1962) 'Classical Electrodynamics' (Wiley: New York).
Komesaroff, M. M. (1970). *Nature* **225**, 612.
Manchester, R. N., Taylor, J. H., and Huguenin, G. R. (1975). *Astrophys. J.* **196**, 83.
Radhakrishnan, V., and Cooke, D. J. (1969). *Astrophys. Lett.* **3**, 225.
Rickett, B. J. (1975). *Astrophys. J.* **197**, 185.
Rickett, B. J., Hankins, T. H., and Cordes, J. M. (1975). *Astrophys. J.* **201**, 425.
Ruderman, M. A., and Sutherland, P. G. (1975). *Astrophys. J.* **196**, 51.
Sieber, W. (1973). *Astron. Astrophys.* **28**, 237.
Taylor, J. H., Manchester, R. N., and Huguenin, G. R. (1975). *Astrophys. J.* **195**, 513.

Manuscript received 17 July 1978